Ultrafast terahertz spectroscopy study of a Kondo insulating thin-film SmB_{6}: Evidence for an emergent surface state

Jingdi Zhang, Jie Yong, Ichiro Takeuchi, Richard L. Greene, and Richard D. Averitt

Phys. Rev. B **97**, 155119 — Published 9 April 2018

DOI: 10.1103/PhysRevB.97.155119

Ultrafast terahertz spectroscopy study of Kondo insulating thin film SmB_6: evidence for an emergent surface state

Jingdi Zhang[1,2*], Jie Yong[3], Ichiro Takeuchi[4], Richard L. Greene[3], Richard D. Averitt[1,2*]

[1] *Department of Physics, Boston University, Boston, Massachusetts, 02215, USA*

[2] *Department of Physics, University of California San Diego, La Jolla, California, 92122, USA*

[3] *Department of Physics, University of Maryland, College Park, Maryland 20742, USA*

[4] *Department of Material Science & Engineering, University of Maryland, College Park, Maryland 20742, USA*

*Correspondence: jdzhang@physics.ucsd.edu; raveritt@ucsd.edu

Abstract:

We utilize terahertz time domain spectroscopy to investigate thin films of the heavy fermion compound SmB_6, a prototype Kondo insulator. Temperature dependent terahertz (THz) conductivity measurements reveal a rapid decrease in the Drude weight and carrier scattering rate at ~T*=20 K, well below the hybridization gap onset temperature (100 K). Moreover, a low-temperature conductivity plateau (below 20 K) suggests the emergence of a surface state with an effective electron mass of 0.1m_e. Conductivity dynamics following optical excitation are also measured and interpreted using Rothwarf-Taylor (R-T) phenomenology, yielding a hybridization gap energy of 17 meV. However, R-T modeling of the conductivity dynamics reveals a deviation from the expected thermally excited quasiparticle density at temperatures below 20 K, indicative of another channel opening up in the low energy electrodynamics. Taken together, these results are consistent with the onset of a surface state well below the crossover temperature (100K) after long-range coherence of the f-electron Kondo lattice is established.

In heavy fermion materials, the strong interaction of *5d* conduction band electrons with a Kondo lattice of localized *4f* electrons renormalizes the Fermi surface (FS), resulting in quasiparticles (QP) with enhanced mass. This interaction also opens up a *d-f* hybridization gap at the Fermi surface, resulting in the formation of a narrow insulating gap. Kondo insulators include SmB_6, YbB_{12}, CeNiSn and spectroscopic techniques including optics have directly observed the hybridization gap [1] [2] [3] [4].

Recent theoretical work has predicted that Kondo insulators are strongly correlated electron systems with the potential to possess a topological non-trivial surface state [5] [6]. The topological surface state emerges due to strong spin-orbit coupling introducing an inversion of the localized 4f band and itinerant 5d bands, a key ingredient for a topological insulator (TI) state [7] [8]. Several experiments on the Kondo insulator SmB_6 have investigated the possibility of a non-trivial topological surface state. This includes transport measurements [9], ARPES [10] [11] [12][13], tunneling spectroscopy [2] [3] [4], and quantum oscillations [14] [15]. Despite a two-dimensional topological surface state, one of the quantum oscillation experiments [15] suggests the existence of a 3D bulk Fermi surface at temperatures ($T < 4$ K) far below the onset temperature (5 K) of conductivity saturation. A strong deviation from the standard Lifshitz-Kosevich behavior of quantum oscillations in SmB_6 has raised a conundrum. Several intriguing proposals, aiming to solve the conundrum include: (i) magnetic breakdown due to a narrow hybridization gap [16], or (ii) a non-conducting bulk Fermi surface, i.e. charge neutral particles [17]. It is likely that SmB_6, as a strongly correlated Kondo insulator in the vicinity of the quantum critical point, posses a non-trivial bulk state at extremely low temperature. It may or may not be independent of the surface state observed at higher

temperatures (T > 1K). This work focuses on the temperature range where the anomalous Fermi surface is not dominant.

Terahertz time-domain spectroscopy (THz-TDS) is a powerful tool to characterize correlated electron materials, providing spectroscopic access to low-energy electrodynamics [18]. Similarly, ultrafast pump-probe spectroscopy has emerged as an indispensable approach to investigate the response of correlated materials upon ultrafast electromagnetic excitation that initiates non-equilibrium dynamics [19]. Femtosecond dynamics measurements are particularly sensitive to the opening of gaps or pseudogaps in numerous materials including heavy fermion materials [20] [21] [22] and superconductors [23]. The dynamics can be phenomenologically analyzed using the Rothwarf-Taylor model to gain insight into the quasiparticle density and recovery dynamics [24] [25]. While many of these experiments have used all-optical pump-probe spectroscopy, which probes the low energy electrodynamics indirectly, the combination of THz spectroscopy with sub-picosecond time resolution (i.e. optical-pump THz-probe (OPTP) spectroscopy [18] [26]) is particularly powerful since the temporal response of the low energy electrodynamics is directly measured.

We utilize terahertz time domain spectroscopy to investigate thin films of the heavy fermion Kondo insulator SmB_6. Both static THz-TDS measurements and dynamic THz conductivity measurements (using OPTP) are reported. THz-TDS conductivity measurements reveal a rapid decrease in the Drude weight and carrier scattering rate at ~20 K, well below the characteristic temperature (100 K) for opening the hybridization gap. The low-temperature residual conductivity below 20 K indicates the emergence of a surface state with an effective electron

mass of $0.1m_e$. Further, the picosecond optical conductivity dynamics exhibit an anomalous amplitude response below 20 K. A Rothwarf-Taylor analysis shows that this behavior arises from a deviation in the thermally excited quasiparticle density expected in a pure single-gap hybridization gap scenario, indicating the opening of an additional channel in the low-temperature electrodynamic response. Our results provide evidence for a crossover from a hybridization gap dominant insulating phase to a surface state dominant regime, suggesting that the onset of a surface state requires long-range coherence of the f-electron Kondo lattice [2].

In our study, preferentially (001) orientated SmB_6 thin films (100 nm thick) were grown by co-sputtering of SmB_6 and B targets in ultrahigh vacuum at 800 ^oC. After in situ annealing of the thin films at the same temperature, the stoichiometry and crystalline orientation was confirmed by wavelength dispersive spectroscopy, TEM and X-ray diffraction [27] [28]. Transport measurements show a resistivity ratio of a factor of two between 2 K and 300 K, due to the emergence of a surface state at low temperatures (**Figure 1 (a)**). **Figure 1(a)** also highlights the different interactions regions in SmB_6 as a function of temperature (as determined from point contact spectroscopy [2]), from weakly interacting around 100K to Kondo lattice hybridization below 20K. **This small resistance ratio is a direct consequence of comparable contribution of surface and bulk conducting channels in thin films of SmB_6.**

A 1 kHz Ti:sapphire regenerative amplifier laser producing 1.55 eV near-infrared pulse (800 nm, 3 mJ, 35 fs) was utilized for these experiments. THz pulses were generated using optical rectification in ZnTe. The THz pulses were used for the temperature dependent THz conductivity measurements and for the OPTP carrier dynamic studies. To measure the THz conductivity of

the sample, the temporal waveform (electric field amplitude and phase) of THz pulse was measured with electro-optic sampling [29]. The complex transmission coefficient in the frequency domain was obtained by taking Fourier transform of the time-domain scans of the THz waveform transmitted through the sample (thin film SmB_6 on MgO substrate) and a reference (a bare MgO substrate). The optical conductivity $\sigma(\omega)$ of the thin film SmB_6 is calculated using the following equation of complex transmission coefficient $\tilde{T}(\omega)$:

$$\tilde{T}(\omega) = \frac{\tilde{E}(\omega)_{sample}}{\tilde{E}(\omega)_{reference}} = \frac{1+\tilde{n}_3}{1+\tilde{n}_3+Z_0\sigma(\omega)d} \exp\left[i\frac{\omega\Delta L}{c}(\tilde{n}_3 - 1)\right]$$

where Z_0 is the free-space impedance (377 Ω), $\tilde{n}_3$ is the refractive index of the substrate and ΔL is the slight difference in thickness between the bare MgO substrate and MgO substrate with the SmB_6 thin film. The quantity ΔL can be precisely calculated from the temporal shift between the sample and reference scans in the time-domain. The conductivity dynamics were measured by adjusting the time delay between 1.55 eV excitation pulses and the THz pulses as described elsewhere [26]. **Figure 1 (b)** schematically displays these experiments in terms of the band structure resulting from d-f hybridization (blue lines) and surface band (red lines). The far-infrared THz pulse (green) interrogates the low energy electrodynamics (bulk and surface). For the dynamic conductivity measurements, an optical pulse (red) creates an excited carrier distribution that rapidly relaxes to the gap edge [20-23].

We first consider the far-infrared response in the absence of photo-excitation. **Figure 2 (a)** plots the frequency dependent complex terahertz conductivity ($\sigma_1 + i\sigma_2$) of thin film SmB_6 at various temperatures. The real THz conductivity (σ_1, below ~1 THz) decreases from 1300 $\Omega^{-1}cm^{-1}$ to a

saturated value of 800 $\Omega^{-1}cm^{-1}$ from 200 K to 4 K, with a conductivity ratio, σ_1(200 K)/σ_1(4 K), of 1.625. This saturation behavior is consistent with DC transport measurements [27] (Fig. 1a), showing a DC conductivity ratio of 1.637. This consistency implies, at low temperature, a surface-state governed electromagnetic response at THz frequencies. The observed decrease in σ_1 is consistent with the opening of the hybridization gap leading to a decrease in the Drude spectral weight. The hybridization gap (HG), however, is at 17 meV (~4.3 THz) and is therefore not spectrally resolved in our measurements (though a slight upturn of the THz conductivity above 1 THz at T < 20 K and the dynamics presented below reveal the effects of the HG). The low temperature conductivity (σ_1 = 800 $\Omega^{-1}cm^{-1}$) may be converted to a 2D sheet conductance of 0.004 Ω^{-1}, consistent with a conductive surface state and sheet resistance given by THz measurement on conventional topological insulators [30] [31].

Figure 2(b) presents a zoomed in view of the frequency dependent imaginary conductivity σ_2 at temperatures from 4 K to 50 K. The linear Drude σ_2 curves clearly fall into two distinct groupings. In the range from 50 to 25 K the data exhibit similar slopes. A sudden increase in the slope below ~ 20 K is observed, accompanied by a sudden rise in σ_2 (110 to 140 $\Omega^{-1}cm^{-1}$ at 0.8 THz [32], see inset of **Figure 2(b)**). This behavior in σ_2 was not observed in previous optical conductivity measurement in single crystal samples [1][33], presumably because the response was dominated by the bulk. The sudden increase in the slope of σ_2 is suggestive of a collapse of the carrier scattering rate γ. In the linear conductivity regime of σ_2 ($\omega\tau \ll 1$, where τ is the carrier scattering time) we can roughly estimate the carrier scattering rate γ by utilizing the equation: $\gamma = \frac{\sigma_1}{\sigma_2}\omega$.

However, a more precise value of γ can be obtained from Drude model fits of the real and imaginary conductivity. In particular, the experimental THz conductivity at T > 25 K (σ_1 and σ_2) is in agreement with a single component Drude oscillator (dashed lines in **Figure 2(a)**). However, below 25 K, σ_1 starts to deviate from the Drude model at higher frequencies (>1 THz). Nonetheless, a single component Drude fit to the low frequency data (< 1 THz) could be used to extract parameters of the free carriers, including the Drude weight (**Figure 2(c)**) and scattering rate (**Figure 2(d)**), even at temperatures below 25K. Recent DC resistivity [27] and magneto-transport measurement [28] on SmB_6 thin films suggest the existence of a conductive surface state. The evidence includes the linear positive magnetoresistance (LPMR) and the nonlinear Hall resistance. The onset temperature of the non-linear Hall resistance coincides with that of the anomaly reported in this work (i.e. ~20K). In addition, STM studies [34] [35] on single crystal SmB_6 show that the surface-state-related density of states (DOS) peak emerges at temperatures below 20 K (but well above the conductivity saturation temperature 5K). Therefore, it is plausible to discuss the anomaly of THz conductivity within the context of the conductive surface state. Although it may be applicable to use other alternative scenarios, such as a 3D unconventional Fermi liquid state in the electrically insulating state observed by quantum oscillation [15], these effects occur at much lower temperature (T < 0.6 K) than the anomaly observed here. In the context of the conductive surface state, it is clear from **Fig. 2(c)** and **(d)** that both the 2D Drude weight ~ $\nu_p^2 t$ (ν_p is the plasma frequency defined as, $\nu_p^2 = \frac{ne^2}{4\pi^2 m^*}$, and t is film thickness) and γ show a marked decrease with temperature. The Drude weight decreases linearly between 100 K and 30 K then decreases by more than 50% between 30 K to 4 K, saturating at 0.057 (THz^2cm). The decrease of $\nu_p^2 t$ below 30 K could be due to a decrease in carrier density or an increase in effective electron mass. This decrease in $\nu_p^2 t$ coincides with the

sharp decrease of the carrier scattering rate from 8 THz to 4 THz between 20 and 30K (**Fig. 2(d)**). A more complete numerical fit that includes an oscillator centered at higher frequency (~20 meV or 5 THz) will require an even larger increase in σ_2 of the Drude component and its slope in the Drude component to compensate the negative contribution due to the high frequency oscillator. The inclusion of an additional high frequency oscillator will cause further decrease of scattering rate of the Drude model. Therefore, a single component Drude fit determines the lower limit for the change in scattering rate and Drude weight, suggesting a radical change in the properties of carriers. This radical change may share the same origin as the anomalies observed by other experiments, probably due to the emergence of the surface state. We now turn to conductivity dynamics measurements, which also reveal anomalous non-Kondo-like behavior below 30 K.

Figure 3(a) displays 1.55 eV photo-excitation induced ultrafast THz conductivity dynamics ($\Delta\sigma$) (or transmission dynamics $\Delta E/E$, where E is the electric field) as a function of time over the temperature range from 60 K to 5 K. The pump fluence was kept below 9 $\mu J/cm^2$ to minimize accumulative thermal heating of the film, confirmed by checking the linearity of the pump-probe dynamics at different fluences. There is an initial increase in the THz conductivity due to photoexcitation of carriers into the conduction band. This is followed by a single exponential relaxation on a picosecond timescale with a flat plateau at longer times. These features are observed in the dynamics at all temperatures investigated. In **Figure 3 (b)**, the data is normalized to the peak, clearly revealing an increase in the photo-excited carrier lifetime as the temperature is decreased. The black lines are fits to the data ($-\Delta E/E = A(T)exp(-t/\tau(T)) + B(T)$). **Figure 3 (c), (d)** plot the lifetime $\tau(T)$ and amplitude $A(T)$ of the fast single-exponential decay dynamics as determined from the fits. The decay time constant increases and then saturates at 10 ps with

decreasing temperature, consistent with opening of the hybridization gap at low temperatures. As for the decay amplitude, upon cooling it first displays a monotonic increase for temperatures above 20K. However, an anomaly occurs below 20K, in accord with the THz-TDS measurements. Instead of reaching monotonically to a saturated amplitude *A(0)*, it decreases by 20% from 20 K to 5 K, in strong contrast to the expected behavior of a single gapped system [25].

The slow down of the single-exponential decay with decreasing temperature arises, in part, from a phonon-bottleneck, characteristic of materials in which an energy gap opens, e.g. superconductors [36] [37], charge density wave materials [38], and Kondo insulators [21]. As the photoexcited quasiparticles relax, collisional processes lead to phonon generation and excitation of electrons across the hybridization gap Δ. The tendency is for electron-hole recombination to decrease the population of photoexcited carriers. However, the nonequilibrium distribution of phonons with energies in excess of Δ (so-called high frequency phonons – HFP) results in additional electron-hole generation that competes with recombination. This is the origin of the phonon-bottleneck. The plateau in the dynamics (**Fig. 3(a)** and **(b)**) arises from this bottleneck with relaxation of the HFP population on a nanosecond timescale governed by anharmonic phonon decay and thermal transport into the substrate. An additional aspect of importance in the relaxation dynamics is the thermally excited carrier density n_T which decreases with temperature in a gapped system. For low-density excitation (as is the case for the present experiments), the thermally excited carriers play an important role in the relaxation, increasing the availability of electrons and holes that can recombine with photogenerated electrons and holes. That is, with decreasing n_T a longer relaxation time is expected as is observed in our SmB_6 films.

The phenomenological *Rothwarf-Taylor* (R-T) model [24] [25] [35] provides a quantitative model to analyze the relaxation dynamics of the photoexcited QPs as heuristically described in the previous paragraph. Specifically, the R-T equations are two coupled differential equations describing the population dynamics of the QPs and HFPs. In the following, we use the R-T model to obtain insight into the underlying physics of the amplitude anomaly. From the temperature dependent single-exponential decay amplitude *A(T)*, we can extract the temperature dependence of the thermally excited carrier (QP) density using

$$n_T = \frac{\eta}{4R}\left[\frac{A(0)}{A(T)} - 1\right] \; or \; n_T \propto \frac{A(0)}{A(T)} - 1 \qquad (1)$$

where R is the recombination rate of electron-hole pairs, η is the electron-hole pair regeneration rate due to annihilation of high frequency phonons (HFP), *A(T)* is the decay amplitude of the QP dynamics, and *A(0)* is the saturated amplitude of single-gapped system at *T=0*. The value of *A(0) = 0.014* is determined by extrapolating the *A(T)* curve from T > 20 K (see **Fig. 3d** dashed line) to zero temperature, corresponding to the expected amplitude in a single gap picture. Intuitively, the amplitude *A(T)* probes the relative change of the optical properties of the sample. It is related to the ratio n_{op}/n_T with the optical excited carrier density given by n_{op} and the equilibrium carrier density given as n_T. The quantity n_{op} is nearly constant (for a given fluence) due to the temperature independent absorption at the excitation wavelength (800 nm, 1.55 eV). Consequently, the temperature dependence of *A(T)* is determined primarily by n_T. Moreover, the R-T model also predicts that the decay rate of pump-probe dynamics follows:

$$\tau^{-1} = \Gamma\left[\frac{\delta}{\varepsilon n_T + 1} + n_T\right] \qquad (2)$$

where $\Gamma = \frac{2R\gamma}{\eta^2\left(1+{}^{2\gamma}/_{\eta}\right)} \approx \frac{2R\gamma}{\eta^2}$ is a temperature independent constant, R and η are defined above and γ is the decay rate of HFP arising from the (i) anharmonic decay of HFP and (ii) diffusion of HFP into the substrate. The coefficient Γ relates the quasi-particle density to the decay rate and the constant δ relates the decay amplitude in the pump-probe dynamics to the photoexcited carrier density. The quantity ε is the inverse of the coefficient $\frac{\eta}{4R}$ in equation (1) with n_T given by the *R-T* model. It takes the general form [24]:

$$n_T \propto T^{1/2}\exp\left(-\Delta/2k_BT\right) \qquad (3)$$

where Δ is the gap energy.

By fitting the decay amplitude and rate (**Figure 4**) simultaneously with Equation (1)-(3), we obtain a Kondo hybridization gap energy of Δ = 17 meV ± 2 meV, consistent with tunneling [2] [3], ARPES [10] [11] [12] and optical conductivity measurements [1]. From **Figure 4b** it is obvious that, despite the agreement of the R-T model with the experiment at T > 20 K, the experimental QP density deviates from n_T = 0 at (T = 0 K), as expected by the R-T model for a single gap scenario. This disagreement with the R-T model cannot be reconciled within the framework of the Kondo hybridization gap, since the thermal excited QP density should be strongly suppressed to zero at low temperatures. In general, the disagreement with R-T model of a single-gapped system indicates opening of additional energy gaps or in-gap states, which re-populate the thermally excited carrier density at low temperature.

Summarizing the results of the static conductivity measurements and the OPTP dynamics, we observe that both experiments reveal an anomalous response below ~20 K. The static THz conductivity starts to approach a saturation value, shows a sudden transition of both 2D Drude weight and scattering rate of carriers around 20 K. The 1.55 eV optical pump-THz probe non-equilibrium dynamics are governed by a pronounced bottleneck behavior consistent with a hybridization gap of 17 meV. More importantly, the thermal quasiparticle density n_T deviates from simple R-T model predictions below 20 K, coinciding with the temperature where a sudden change of the Drude weight and scattering rate is observed. In short, the Kondo insulator SmB_6 thin films enters a regime where the hybridization gap is insufficient to describe the electrodynamic response below T* = 20 K.

We suggest that the anomalies observed at T* arise from the activation of the conductive surface state and the coherent Kondo lattice, which has also been observed in point contact spectroscopy (PCS) experiment on single crystal SmB_6 [2]. PCS experiments suggest that, although the hybridization gap opens up at temperatures up to 100 K, inter-ion correlation emerges at temperature below ~ 30 K, which is close to the T* we observe. To obtain insight to the surface state, we use the low temperature carrier density of the surface state ~2×10^{14} cm^{-2} reported by quantum oscillation (QO) studies [14] to estimate the electron effective mass. Using the QO carrier density with the THz 2D Drude weight, we obtain an electron effective mass of $m^* = 0.1m_e$, consistent with theoretical work [39] reporting a much lighter surface state quasiparticle as a result of Kondo breakdown (KB). This further indicates that the residual THz conductivity (v<1 THz) at low temperature is due to a surface state.

We speculate that Kondo coherence state plays a crucial role in the observed electrodynamic anomalies. The onset temperature of the coherent Kondo state [2] is coincides with T* in our experiments, hinting that Kondo state coherence is a prerequisite for the emergence of the surface state. This suggests that at T* a macroscopic surface state emerges and competes with the bulk. This is consistent with the onset temperature of 2D surface state signature in quantum oscillation data [14] and STM results [34][35]. It remains to reconcile these results with ARPES experiments where the electronic band corresponding to surface state emerges at the temperature T_K when hybridization gap opens up.

To conclude, static THz conductivity experiments and ultrafast conductivity measurements display anomalies below a characteristic temperature T* = 20K strongly indicating the emergence of a surface state that may require the formation of a coherent Kondo lattice for its existence.

Acknowledgement: The authors would like to acknowledge Congjun Wu, Gu-Feng Zhang, Xiangfeng Wang, Tao Wu and Xianhui Chen for valuable discussions. JZ and RDA acknowledge support from DOE - Basic Energy Sciences under Grant No. DE-FG02-09ER46643 and DE-SC0012375, under which the THz measurements and data analysis were performed. JY, IT and RLG acknowledge support from ONR N00014-13-1-0635 and NSF DMR 1410665.

References:

[1] B. Gorshunov, N. Sluchanko, A. Volkov, M. Dressel, G. Knebel, A. Loidl, and S. Kunii, Phys. Rev. B **59**, 1808 (1999).

[2] X. Zhang, N. P. Butch, P. Syers, S. Ziemak, R. L. Greene, and J. Paglione, Phys. Rev. X **3**, 011011 (2013).

[3] W. Ruan, C. Ye, M. Guo, F. Chen, X. Chen, G.-M. Zhang, and Y. Wang, Phys. Rev. Lett. **112**, 136401 (2014).

[4] M. M. Yee, Y. He, A. Soumyanarayanan, D.-J. Kim, Z. Fisk, and J. E. Hoffman, arXiv Preprint arXiv:1308.1085 (2013).

[5] M. Dzero, K. Sun, V. Galitski, and P. Coleman, Phys. Rev. Lett. **104**, 106408 (2010).

[6] F. Lu, J. Z. Zhao, H. Weng, Z. Fang, and X. Dai, Phys. Rev. Lett. **110**, 096401 (2013).

[7] M. Z. Hasan and C. L. Kane, Reviews of Modern Physics **82**, 3045 (2010).

[8] X.-L. Qi and S.-C. Zhang, Reviews of Modern Physics **83**, 1057 (2011).

[9] D.-J. Kim, J. Xia, and Z. Fisk, Nature Materials **13**, 466 (2014).

[10] J. Jiang, S. Li, T. Zhang, Z. Sun, F. Chen, Z. R. Ye, M. Xu, Q. Q. Ge, S. Y. Tan, X. H. Niu, and others, Nature Communications **4**, 3010 (2013).

[11] M. Neupane, N. Alidoust, S. Xu, T. Kondo, Y. Ishida, D.-J. Kim, C. Liu, I. Belopolski, Y. J. Jo, T.-R. Chang, and others, Nature Communications **4**, 2991 (2013).

[12] N. Xu, P. K. Biswas, J. H. Dil, R. S. Dhaka, G. Landolt, S. Muff, C. E. Matt, X. Shi, N. C. Plumb, M. Radović, and others, Nature Communications **5**, 4566 (2014).

[13] N. Xu, C. E. Matt, E. Pomjakushina, X. Shi, R. S. Dhaka, N. C. Plumb, M. Radović, P. K. Biswas, D. Evtushinsky, V. Zabolotnyy, J. H. Dil, K. Conder, J. Mesot, H. Ding, and M. Shi, Phys. Rev. B **90**, 085148 (2014).

[14] G. Li, Z. Xiang, F. Yu, T. Asaba, B. Lawson, P. Cai, C. Tinsman, A. Berkley, S. Wolgast, Y. S. Eo, and others, Science **346**, 1208 (2014).

[15] B. S. Tan, Y.-T. Hsu, B. Zeng, M. Ciomaga Hatnean, N. Harrison, Z. Zhu, M. Hartstein, M. Kiourlappou, A. Srivastava, M. D. Johannes, T. P. Murphy, J.-H. Park, L. Balicas, G. G. Lonzarich, G. Balakrishnan, Suchitra E. Sebastian, Science **349**, 287 (2015).

[16] O. Erten, P. Ghaemi and P. Coleman, Phys. Rev. Lett. **116**, 046403 (2016).

[17] G. Baskaran, arXiv:1507.03477 (2015).

[18] D. N. Basov, R. D. Averitt, D. van der Marel, M. Dressel, and K. Haule, Reviews of Modern Physics **83**, 471 (2011).

[19] J. Zhang and R. D. Averitt, Annual Review of Materials Research **44**, 19 (2014).

[20] J. Demsar, R. D. Averitt, K. H. Ahn, M. J. Graf, S. A. Trugman, V. V. Kabanov, J. L. Sarrao, and A. J. Taylor, Phys. Rev. Lett. **91**, 027401 (2003).

[21] J. Demsar, V. K. Thorsmolle, J. L. Sarrao, and A. J. Taylor, Phys. Rev. Lett. **96**, 037401 (2006).

[22] S. Adhikari, Y. Ma, Z. Fisk, J. Xia, C.B. Eom, C. Cen, arXiv:1502.04441 (2015).

[23] J. Demsar, R. D. Averitt, A. J. Taylor, V. V Kabanov, W. N. Kang, H. J. Kim, E. M. Choi, and S. I. Lee, Phys. Rev. Lett. **91**, 267002 (2003).

[24] A. Rothwarf and B. N. Taylor, Phys. Rev. Lett. **19**, 27 (1967).

[25] V. V. Kabanov, J. Demsar, and D. Mihailovic, Phys. Rev. Lett. **95**, 147002 (2005).

[26] R. A. Kaindl and R. D. Averitt, in *Terahertz Spectroscopy Principles and Applicaitions*, edited by S. L. Dexheimer (CRC press, 2007), pp. 119–170.

[27] J. Yong, Y. Jiang, D. Usanmaz, S. Curtarolo, X. Zhang, L. Li, X. Pan, J. Shin, I. Takeuchi, and R. L. Greene, Applied Physics Letters **105**, 222403 (2014).

[28] J. Yong, Y. Jiang, X. Zhang, J. Shin, I. Takeuchi, and R. L. Greene, AIP Advances **5**, 077144 (2015).

[29] Q. Wu and X.-C. Zhang, Applied Physics Letters **67**, 3523 (1995).

[30] R. Valdes Aguilar, A. V Stier, W. Liu, L. S. Bilbro, D. K. George, N. Bansal, L. Wu, J. Cerne, A. G. Markelz, S. Oh, and N. P. Armitage, Phys. Rev. Lett. **108**, 087403 (2012).

[31] K. W. Post, B. C. Chapler, M. K. Liu, J. S. Wu, H. T. Stinson, M. D. Goldflam, A. R. Richardella, J. S. Lee, A. A. Reijnders, K. S. Burch, M. M. Fogler, N. Samarth, and D. N. Basov, Phys. Rev. Lett. **115**, 116804 (2015).

[32] We Choose 0.8 THz, Because the Sensitivity of THz Conductivity in Current Experiment Peaks at 0.8 THz (n.d.).

[33] N. J. Laurita, C. M. Morris, S. M. Koohpayeh, P. F. S. Rosa, W. A. Phelan, Z. Fisk, T. M. McQueen, and N. P. Armitage, Phys. Rev. B **94**, 165154 (2016).

[34] L. Jiao, S. Rößler, D. J. Kim, L. H. Tjeng, Z. Fisk, F. Steglich, and S. Wirth, Nat. Commun. **7**, 13762 (2016).

[35] W. K. Park, L. Sun, A. Noddings, D.-J. Kim, Z. Fisk, and L. H. Greene, Proc. Natl. Acad. Sci. **113**, 201606042 (2016).

[36] R. D. Averitt, G. Rodriguez, A. I. Lobad, J. L. W. Siders, S. A. Trugman, and A. J. Taylor, Phys. Rev. B **63**, 140502 (2001).

[37] N. Gedik, P. Blake, R. C. Spitzer, J. Orenstein, R. Liang, D. A. Bonn, and W. N. Hardy, Phys. Rev. B **70**, 014504 (2004).

[38] J. Demsar, K. Biljakovic, and D. Mihailovic, Phys. Rev. Lett. **83**, 800 (1999).

[39] V. Alexandrov, P. Coleman, and O. Erten, Phys. Rev. Lett. **114**, 177202 (2015).

Figure Captions:

Figure 1 (color online). **(a)** Temperature dependent DC resistivity of SmB_6 thin film. Regions of different color indicate regimes that *d* electrons interact differently with local *f* electrons as determined by point contact spectroscopy [2]. **(b)** Schematic of THz spectroscopy of Kondo insulator SmB_6. Green arrows indicate low energy excitations that are probed by THz pulse. The 800 nm near-IR pulse initiates ultrafast non-equilibrium dynamics by creating an excited quasiparticle distribution that subsequently relaxes.

Figure 2 (color online). **(a)** Real and imaginary THz conductivity (experiment, solid lines; Drude fit, dash and dotted lines, for real and imaginary part, respectively) at different temperatures (4 K to 200 K). Triangles label the scattering rate of carriers at each temperature. **(b)** Imaginary part of THz conductivity in the temperature range (4 K to 50K). Inset shows σ_{imag} at 0.8 THz in the temperature range from 4 to 100 K. **(c)** Temperature dependence of Drude weight. **(d)** Temperature dependence of carrier scattering rate.

Figure 3 (color online). **(a)** Optical (1.55 eV) pump-THz probe dynamics (experiment, thick colored lines; single-exponential fit, thin black lines) of SmB_6 thin films from 5 K to 60 K, showing the photo-induced change in transmission (left y-axis) and THz conductivity (right y-axis). **(b)** Normalized pump-probe traces at various temperatures. **(c), (d)** Temperature dependence of the single-exponential decay constant and amplitude. Solid line in **(d)** indicates the temperature dependent decay amplitude predicated by ideal single-gap Rothwarf-Taylor model.

Figure 4 (color online). Rothwarf-Taylor model fitting (solid curve) to **(a)** the single-exponential decay rate and **(b)** thermal excited carrier density n_T.

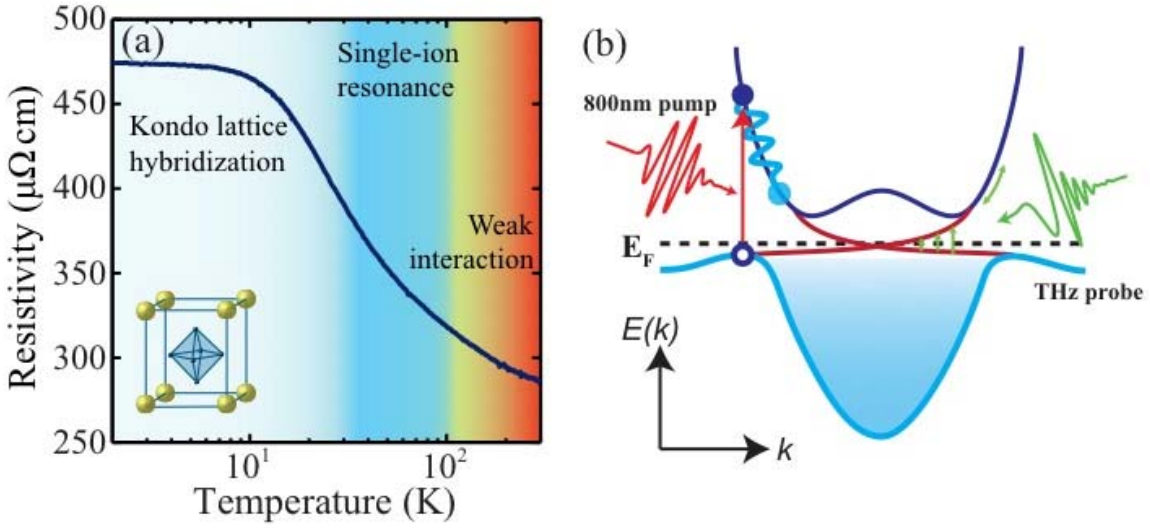
(a)
Single-ion
resonance
Kondo lattice
hybridization
Weak
interaction
Resistivity (μΩ cm)
500
450
400
350
300
250
10^1
10^2
Temperature (K)
(b)
800nm pump
E_F
THz probe
E(k)
k

Figure 1

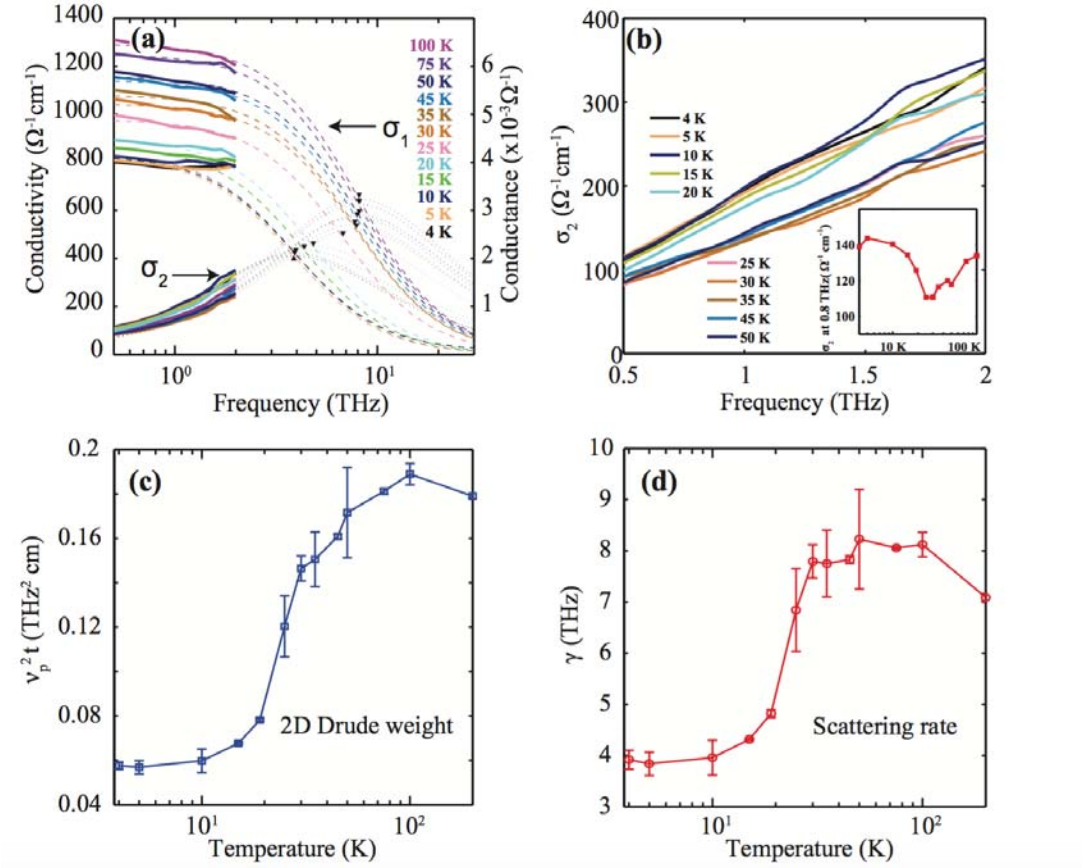
(a)
100 K
75 K
50 K
45 K
35 K
30 K
25 K
20 K
15 K
10 K
5 K
4 K
σ1
σ2
Conductivity (Ω-1cm-1)
Conductance (x10-3Ω-1)
Frequency (THz)
(b)
4 K
5 K
10 K
15 K
20 K
25 K
30 K
35 K
45 K
50 K
σ2 (Ω-1cm-1)
Frequency (THz)
(c)
2D Drude weight
vp2 t (THz2 cm)
Temperature (K)
(d)
Scattering rate
γ (THz)
Temperature (K)

Figure 2

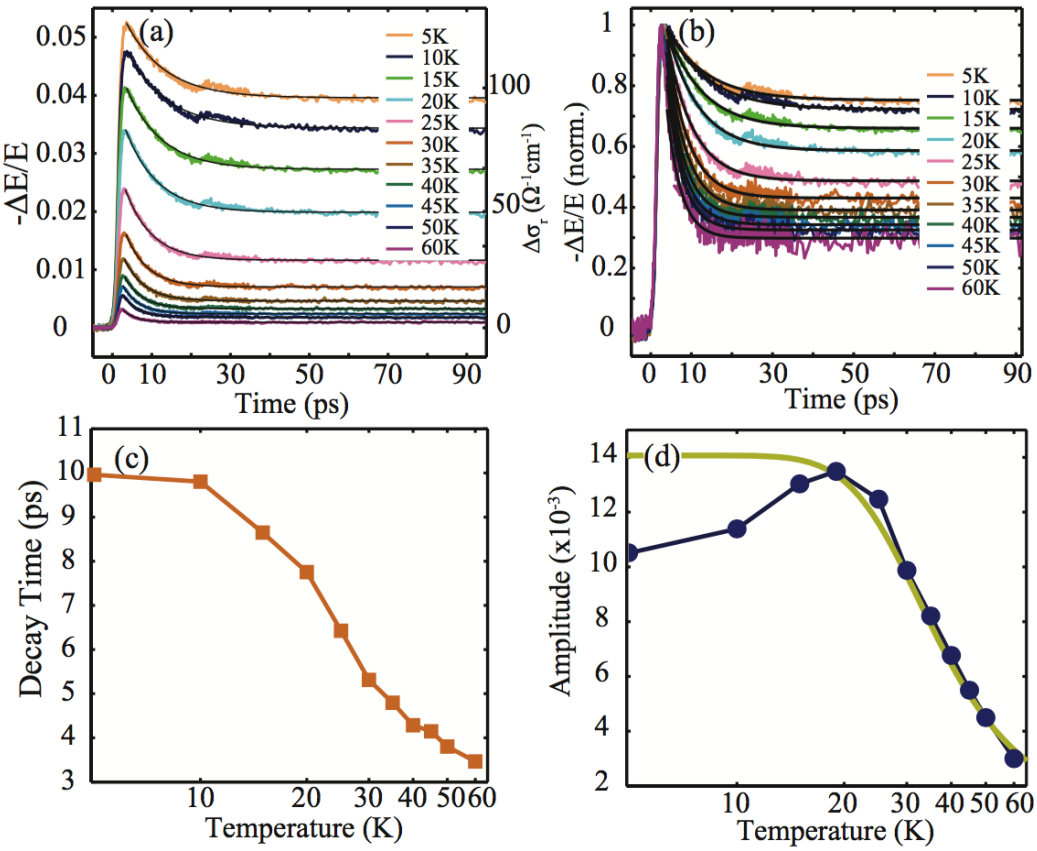
(a)
(b)
(c)
(d)
5K
10K
15K
20K
25K
30K
35K
40K
45K
50K
60K
-ΔE/E
Δσr (Ω-1cm-1)
-ΔE/E (norm.)
Time (ps)
Decay Time (ps)
Amplitude (x10-3)
Temperature (K)

Figure 3

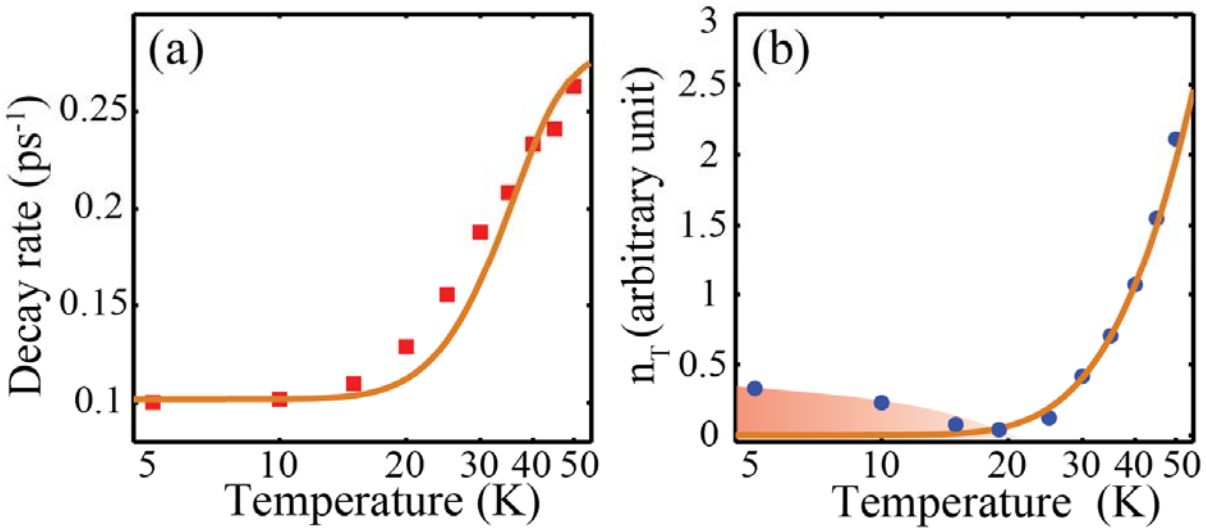
(a)
Decay rate (ps^{-1})
0.25
0.2
0.15
0.1
5
10
20
30
40
50
Temperature (K)
(b)
n_T (arbitrary unit)
3
2.5
2
1.5
1
0.5
0
5
10
20
30
40
50
Temperature (K)

Figure 4